Analytical Methods

ROYAL SOCIETY OF CHEMISTRY

PAPER

View Article Online
View Journal | View Issue

Cite this: *Anal. Methods*, 2026, **18**, 2799

Waste to resource approach: $CoFe_2O_4$-modified spent tea waste for magnetic solid-phase extraction of toxic metal ions from water samples

Serdal Seker,[a] Duygu Ozdes *[b] and Celal Duran [c]

In this research, within the framework of a waste-to-resource conversion approach, biochar obtained from spent tea waste (STWB), a widely available and cost-free biomass source, was modified with magnetic $CoFe_2O_4$ nanoparticles to develop an environmentally friendly adsorbent ($CoFe_2O_4$/STWB). The applicability of this material for efficient separation and preconcentration of Cd(II), Pb(II), and Ni(II) ions from mining wastewater, stream water, and wastewater samples collected from an organized industrial zone was systematically investigated using the solid phase extraction (SPE) method. Optimization of the experimental variables was conducted to enhance the extraction performance of the target analyte ions. The fact that the adsorption and desorption equilibrium times occur in less than 1 min demonstrates the rapid and highly efficient extraction performance of the developed adsorbent. Langmuir isotherm model analysis revealed that $CoFe_2O_4$/STWB exhibits adsorption capacities of 69.4 mg g^{-1} for Cd(II), 185.2 mg g^{-1} for Pb(II), and 45.2 mg g^{-1} for Ni(II). In contrast, the corresponding adsorption capacities obtained for unmodified STWB were considerably lower, with values of 42.9, 75.8, and 16.8 mg g^{-1} for Cd(II), Pb(II), and Ni(II), respectively. These results clearly demonstrate that modification with $CoFe_2O_4$ significantly enhances the adsorption performance of STWB. Consequently, $CoFe_2O_4$-modified spent tea waste can be regarded as an effective, economical, and sustainable adsorbent for trace heavy metal analysis in environmental water samples, owing to its rapid extraction kinetics, high adsorption capacity, and low detection limits.

Received 26th January 2026
Accepted 8th March 2026

DOI: 10.1039/d6ay00152a

rsc.li/methods

1 Introduction

Heavy metals (HMs) represent a major class of environmental contaminants owing to their pronounced toxicity, tendency to bioaccumulate, and resistance to degradation in environmental systems.[1] Heavy metal ions such as cadmium (Cd), lead (Pb), and nickel (Ni) can enter aquatic environments through mining activities, metal plating industries, battery and accumulator production, paint and pigment manufacturing, fertilizer application, and the discharge of domestic and industrial wastewater.[2] Even at low concentrations, these metals exert serious toxic effects on living organisms; Cd is associated with kidney and bone damage,[3] Pb can cause disorders of the nervous system and developmental impairments,[4] while Ni may induce allergic reactions, respiratory diseases, and an increased risk of cancer.[5] Therefore, the precise and reliable determination of HM levels in drinking and surface waters is of great importance for environmental monitoring and the protection of public health.[6]

In the analysis of HMs in environmental matrices, the presence of metal ions at very low concentrations, along with matrix interferences, often complicates analytical measurements. Therefore, the application of a preconcentration step prior to direct analysis is of great importance.[7] Commonly employed preconcentration techniques include liquid–liquid extraction,[8] cloud point extraction,[9] solid-phase extraction,[10] and coprecipitation.[11] Among these methods, SPE has gained particular prominence due to its ability to provide high preconcentration factors, low solvent consumption, reusability of adsorbents, ease of automation, and environmentally friendly characteristics.[12] SPE is an efficient preconcentration method based on the selective retention of target analytes on a suitable adsorbent, followed by their recovery using a small volume of eluent.[13] When magnetic adsorbents are integrated into SPE systems, the need for centrifugation or filtration is eliminated, resulting in a significant reduction in processing time. Magnetic solid-phase extraction (MSPE) enables the improvement of detection limits, particularly in metal analyses performed using techniques with relatively low sensitivity, such as flame atomic absorption spectrometry (FAAS).[14]

[a]*Gumushane University, Graduate School of Education, Gumushane, 29100, Türkiye*
[b]*Gumushane University, Gumushane Vocational School, 29100, Gumushane, Türkiye. E-mail: duyguozdes@gumushane.edu.tr*
[c]*Karadeniz Technical University, Faculty of Sciences, Department of Chemistry, 61080, Trabzon, Türkiye*

In recent years, research has increasingly concentrated on the development of environmentally friendly, low-cost, and sustainable adsorbents that can be effectively employed in SPE techniques. Biochar is a carbonaceous substance obtained *via* pyrolysis of biomass-derived resources under oxygen-limited or oxygen-free conditions. Its production from agricultural and organic wastes, together with its high specific surface area and abundant surface functional groups, makes it a highly attractive adsorbent for environmental applications.[15,16] Accordingly, the conversion of abundant biomass resources commonly regarded as waste—such as spent tea waste—into biochar provides significant advantages in terms of waste valorization and the generation of value-added materials.[17] In the existing literature, biochar has been extensively used as a sorbent for the separation and preconcentration of organic contaminants using SPE. Yang *et al.* reported the use of wolfberry biomass waste derived biochar as a SPE sorbent, enabling efficient extraction of 26 antibiotics from aquatic products.[18] Niu *et al.* developed a SPE method utilizing eco-friendly coconut shell biochar as the adsorbent for the extraction and quantification of phenoxyacetic acid herbicides in environmental matrices.[19]

Surface modification has been widely applied in numerous studies to enhance the adsorption capacity and separation efficiency of biochars. In particular, modifying biochar with magnetic nanoparticles provides significant advantages by improving adsorption properties as well as enabling rapid and efficient phase separation with the assistance of an external magnetic field.[20–22] Among various magnetic materials, spinel-structured $CoFe_2O_4$ magnetic nanoparticles are frequently preferred for adsorbent modification owing to their high specific surface area, well-developed porosity, excellent sorption capability, non-toxic nature, insolubility in water, cost-effectiveness, excellent phase stability, and strong resistance to corrosion.[23,24] When biochar-based structures are modified with $CoFe_2O_4$, they can establish strong interactions with heavy metal ions *via* mechanisms including electrostatic attraction, surface complexation, and ion exchange, thereby acting as efficient adsorbents in analytical applications.[25,26] Shabelskaya *et al.* reported a one-step synthesis of $CoFe_2O_4$/biochar composites derived from agricultural waste, demonstrating high adsorption efficiency toward Cr(VI) removal from aqueous solutions.[27] Ozdes and Duran developed a $CoFe_2O_4$-modified melon peel biochar for MSPE, achieving rapid and sensitive FAAS analysis of Cu(II), Cd(II), and Pb(II) in environmental and food samples.[17]

In this study, biochar obtained from spent tea waste was modified with $CoFe_2O_4$ magnetic nanoparticles, and the resulting $CoFe_2O_4$-modified biochar was employed, for the first time, as an adsorbent for the preconcentration of Cd(II), Pb(II), and Ni(II) ions from aqueous media *via* MSPE. In the context of this research, experimental parameters affecting adsorption and desorption efficiencies were optimized, and the obtained data were evaluated using various adsorption isotherm models. Accuracy of the developed procedure was verified through spike-recovery experiments by adding known amounts of analytes to water sample matrices. According to the literature, there is no report on the application of biochar derived from spent tea waste modified with magnetic nanoparticles ($CoFe_2O_4$) for the recovery of heavy metals *via* the SPE method. In this respect, the present study offers an environmentally friendly approach by developing a novel adsorbent system and converting waste biomass into high value-added products.

2 Materials and methods

2.1 Chemicals and instrumentation

All reagents employed throughout the experimental procedures, including nitric acid (HNO_3), sodium hydroxide (NaOH), hydrochloric acid (HCl), iron(III) chloride hexahydrate ($FeCl_3 \cdot 6H_2O$), cobalt(II) nitrate hexahydrate ($Co(NO_3)_2 \cdot 6H_2O$), and the salts employed in interference studies (NaCl, KCl, $Ca(NO_3)_2$, $Mg(NO_3)_2$, Na_2CO_3, $NaNO_3$, Na_3PO_4, Na_2SO_4, and NH_4Cl), were of analytical grade and purchased from Sigma-Aldrich (Shanghai, China) and Merck (Darmstadt, Germany). The reagents were used without further purification. Cd(II), Pb(II), and Ni(II) stock solutions (1000 mg L^{-1}) were prepared in HNO_3, and subsequent working solutions were obtained by diluting them with distilled water. Before use, all glassware was immersed in 5% (v/v) HNO_3 overnight and subsequently rinsed with tap water and distilled water to remove any residual contaminants.

Scanning electron microscopy coupled with energy-dispersive X-ray spectroscopy (SEM-EDX) analysis (ZEISS SIGMA 300) was performed to assess the surface morphology and elemental composition of STWB and $CoFe_2O_4$/STWB. Fourier-transform infrared (FTIR) spectroscopy was implemented through a PerkinElmer Spectrum Two device to characterize the surface functional groups. XRD patterns of the adsorbents were obtained employing Cu Kα radiation (λ = 1.5406 Å) over 2θ = 5–80° on a PANalytical X'Pert3 powder diffractometer. N_2 adsorption–desorption isotherms at 77 K were used to determine the specific surface area and porosity of the adsorbents *via* the BET method.

Determination of metal ion concentrations was conducted through a flame atomic absorption spectrometer (PerkinElmer AAnalyst 400). A WTW inoLab pH 7110 benchtop pH meter was used for pH adjustment and measurement. Adsorption experiments were conducted using a BOECO PSU-15i mechanical shaker, and a NUVE NF 200 centrifuge was employed for phase separation. An analytical balance (KERN ABJ 220-4NM) was used for weighing the adsorbents and chemicals, while magnetic stirring was carried out using an IKA RCT Basic stirrer. A Weightlab WF-UD6 ultrasonic bath was used during the synthesis of $CoFe_2O_4$, and calcination was performed in a Protech muffle furnace. Drying of the adsorbents was carried out in a Santen SE 125 drying oven.

2.2 Preparation of $CoFe_2O_4$ modified spent tea waste-derived biochar ($CoFe_2O_4$/STWB)

In order to obtain biochar from spent tea waste, the tea residue was first dried in an oven at 105 °C and then placed in a lidded crucible inside a muffle furnace. Subsequently, the material was heated to 500 °C under an oxygen-limited atmosphere, and

biochar (STWB) was produced through a pyrolysis process maintained at this temperature for 2 h.

The modification of spent tea waste biochar with $CoFe_2O_4$ magnetic nanoparticles was carried out based on the co-precipitation method proposed by Lai *et al.* with slight modifications.[28] Briefly, Fe^{3+} and Co^{2+} ions were weighed from $FeCl_3 \cdot 6H_2O$ and $Co(NO_3)_2 \cdot 6H_2O$ salts at a molar ratio of 2 : 1 and mixed with 7.0 g of STWB. Subsequently, 250 mL of deionized water was added, and the resulting suspension was stirred on a magnetic stirrer at 35–40 °C for 30 min. After magnetic stirring, the suspension was placed in an ultrasonic bath and maintained at 80 °C for 2 h. To adjust the pH in the range of 10–11, a dropwise addition of preheated 3 M NaOH solution (80 °C) was carried out into the suspension. Following NaOH addition, the system was kept at 80 °C for a further 30 min. The resulting precipitate was cooled to room temperature and isolated by filtration. The precipitate was repeatedly rinsed with deionized water until the pH approached neutrality. After washing, the magnetic biochar was dried in an oven at 105 °C for 6 h and subsequently calcined at 400 °C for 4 h. Finally, the obtained magnetic biochar was ground into a fine powder using a porcelain mortar and stored in plastic containers.

2.3 Adsorption and desorption of analyte ions

The SPE experiments were carried out using a batch method. In this procedure, 10 mL aqueous solutions containing 5.0 μg of Cd(II), 20.0 μg of Pb(II), and 10.0 μg of Ni(II) ions, along with 25 mg of the adsorbent, were transferred into centrifuge tubes. The pH of the solutions was adjusted to 6.0 using dilute HCl and NaOH. The prepared mixtures were shaken on a mechanical shaker for 1 min and then either centrifuged at 3000 rpm for 2 min or subjected to an external magnetic field to settle the $CoFe_2O_4$/STWB adsorbent, which had adsorbed the analyte ions, at the bottom of the tube. The supernatant was removed by decantation. For desorption of the analyte ions, the adsorbent collected at the bottom of the tube was treated with 5.0 mL of 0.2 M HCl solution for 1 min. Following this step, the mixture was centrifuged again under the same conditions. The concentrations of Cd(II), Pb(II), and Ni(II) ions transferred into the aqueous phase were then determined by FAAS.

2.4 Preparation of water samples

The $CoFe_2O_4$/STWB-based SPE method was employed for the analysis of mining wastewater, stream water (Harşit Stream, Gümüşhane), and wastewater collected from an organized industrial zone. The water samples were filtered through a cellulose nitrate membrane (0.45 μm) immediately after collection, acidified with 1% (v/v) HNO_3 to inhibit microbial activity, and stored in polyethylene bottles until analysis.

3 Results and discussion

3.1 Adsorbent synthesis and characterization

3.1.1 Functional group analysis by FTIR. In the FTIR spectrum of STWB (Fig. 1), the broad band in the 3600–3000 cm^{-1} region is attributed to O–H stretching vibrations of hydroxyl groups (–OH) in alcohols and phenolic compounds within the biochar structure. The band at 1581 cm^{-1} is assigned to asymmetric stretching vibrations of carboxylate (COO^-) groups or C=C stretching of aromatic rings, while the band at 1410 cm^{-1} corresponds to symmetric carboxylate stretching or C=C vibrations of aromatic structures.[29,30] The band observed around 1325 cm^{-1} is related to C–H bending vibrations, indicating the presence of aliphatic or aromatic hydrocarbon bonds in the organic structure.[31] The band at 1134 cm^{-1} arises from C–O stretching vibrations in compounds such as ethers or phenols.[32] In addition, the sharp bands detected at 875 cm^{-1}, 810 cm^{-1}, and 751 cm^{-1} can be assigned to out-of-plane bending vibrations of aromatic C–H bonds in benzene derivatives.[33]

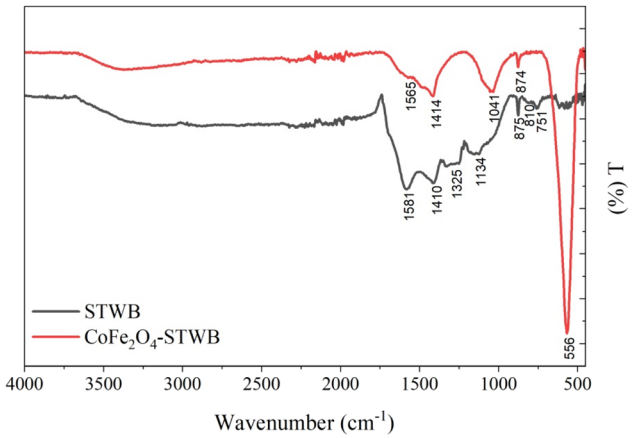

Fig. 1 FTIR spectra of STWB and $CoFe_2O_4$/STWB.

As shown in Fig. 1, the FTIR spectra of STWB and $CoFe_2O_4$/STWB reveal noticeable changes in both band positions and intensities following the modification process. Slight shifts in the positions of several characteristic bands, along with significant variations in band intensities, were observed, which can be attributed to the interactions between $CoFe_2O_4$ nanoparticles and the functional groups present on the biochar surface. In particular, the distinct band appearing at 567 cm^{-1}, assigned to Fe–O stretching vibrations, confirms the successful loading of $CoFe_2O_4$ nanoparticles onto the biochar surface and verifies the effective modification process.[34]

3.1.2 Morphological analysis by SEM-EDX. SEM analysis was employed to examine the surface morphology of STWB and $CoFe_2O_4$/STWB, to identify changes in surface topography after modification, and to evaluate the distribution of $CoFe_2O_4$ nanoparticles on the biochar surface, while EDX analysis was used to assess the elemental composition of STWB and $CoFe_2O_4$/STWB adsorbents. Fig. 2 presents the SEM images of STWB and $CoFe_2O_4$/STWB adsorbents. Examination of the STWB surface reveals that the adsorbent exhibits a relatively smooth, layered structure with low porosity (Fig. 2(a)). Following magnetic modification, pronounced changes in surface morphology were observed, characterized by the widespread distribution of spherical, high-contrast $CoFe_2O_4$ nanoparticles on the carbonaceous matrix (Fig. 2(b)). This

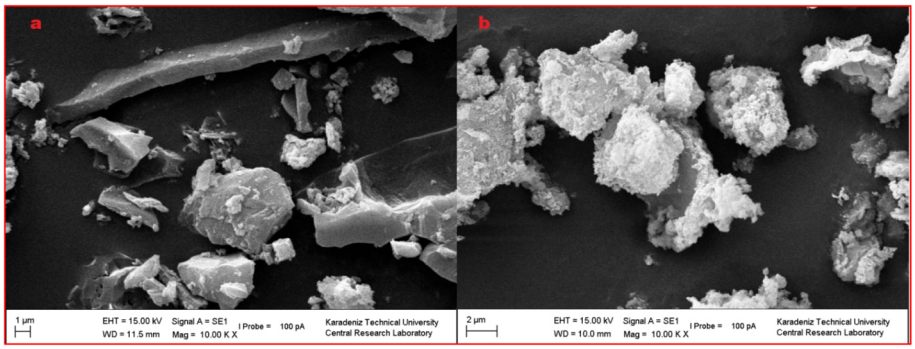

Fig. 2 SEM images of (a) STWB and (b) $CoFe_2O_4$/STWB.

morphological transformation indicates that the $CoFe_2O_4$ phase was successfully anchored onto the biochar surface. Moreover, the increased surface roughness resulting from nanoparticle loading suggests the formation of new potential active sites for adsorption, which is expected to improve the adsorption efficiency of the modified adsorbent.

According to the EDX analysis results of STWB presented in Fig. 3(a), the material is mainly composed of carbon (69 wt% C) and oxygen (22 wt% O), which is consistent with its lignocellulosic origin. In addition, nitrogen (5 wt% N) and sulfur (5 wt% S) were detected at lower proportions in the biochar structure. The presence of these heteroatoms indicates that the biochar surface contains various functional groups that may contribute to metal ion binding. In the EDX spectrum shown in Fig. 3(b), the detected cobalt (8 wt% Co) and iron (21 wt% Fe) contents clearly demonstrate the successful incorporation of $CoFe_2O_4$ components onto the biochar surface. In parallel with the presence of the metal oxide structure, the relative surface oxygen content increased to 51 wt%, while the carbon content decreased to approximately 10 wt%, owing to surface coverage by magnetic nanoparticles. These findings collectively confirm that the biochar surface was effectively and successfully modified with magnetic $CoFe_2O_4$ nanoparticles.

3.1.3 Structural analysis by XRD. The XRD diffractogram of the $CoFe_2O_4$/STWB composite presented in Fig. 4 reveals distinct diffraction peaks at 2θ values of 30.10°, 35.64°, 43.10°, 53.56°, 57.46°, and 62.83°. These characteristic reflections correspond to the (220), (311), (400), (422), (511), and (440) crystal planes of the cubic spinel $CoFe_2O_4$ phase, respectively, and show excellent agreement with the standard JCPDS card no. 22-1086. The findings confirm the formation of crystalline $CoFe_2O_4$ nanoparticles on STWB, demonstrating that the magnetic modification was successful.

3.1.4 Surface area analysis by the BET method. The BET surface area (S_{BET}) of STWB was determined to be 6.02 $m^2\ g^{-1}$, while the surface area of the $CoFe_2O_4$/STWB nanomaterial

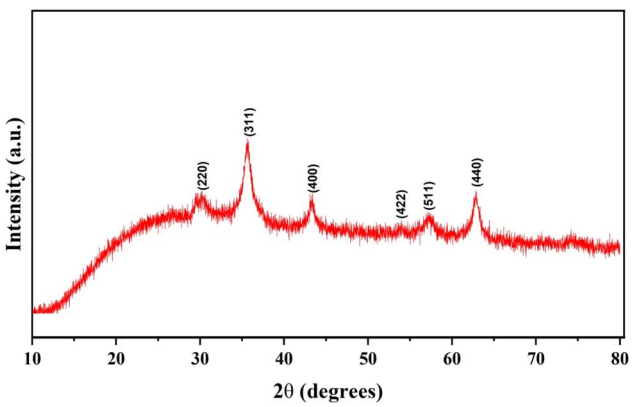

Fig. 4 XRD pattern of $CoFe_2O_4$/STWB.

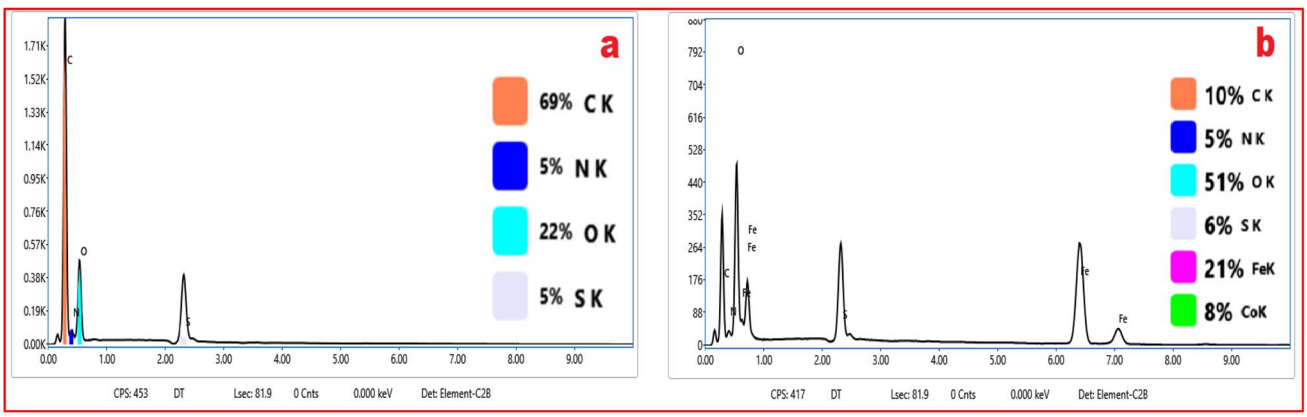

Fig. 3 EDX analyses of (a) STWB and (b) $CoFe_2O_4$/STWB.

significantly increased to 64.9 m^2 g^{-1}. This substantial enhancement indicates that the structure has become more porous due to the successful attachment of $CoFe_2O_4$ nanoparticles to the STWB surface. Furthermore, while the total pore volume of STWB was immeasurable, this value was obtained as 0.179 cm^3 g^{-1} for $CoFe_2O_4$/STWB. The obtained results reveal that magnetic modification markedly improves the surface and pore characteristics of the adsorbent, and consequently, an increase in adsorption performance is expected.

3.1.5 Interaction mechanism between $CoFe_2O_4$ and STWB. During the *in situ* co-precipitation process under alkaline conditions, Fe^{3+} and Co^{2+} species undergo hydrolysis and subsequently nucleate in the presence of STWB. Because ferrite formation occurs directly within the biochar suspension, the biochar surface may serve as a platform for heterogeneous nucleation and growth of $CoFe_2O_4$ nanoparticles rather than simple physical mixing. The oxygen-containing functional groups of STWB (such as hydroxyl and carboxyl groups) are expected to act as anchoring sites for metal species, thereby contributing to nanoparticle immobilization through interfacial metal–oxygen interactions.[34,58] This interpretation is supported by the observed shifts and intensity changes in FTIR bands of the composite compared to those of pristine STWB, indicating possible involvement of surface functional groups during ferrite formation. Moreover, XRD patterns confirm the successful formation of the crystalline spinel $CoFe_2O_4$ phase within the composite structure. The coexistence of characteristic biochar features and distinct $CoFe_2O_4$ diffraction peaks suggests the formation of a structurally integrated magnetic composite rather than a simple physical mixture.

3.2. Adsorption study

3.2.1 Influence of pH on the adsorption/extraction of target metal ions. The solution pH directly influences metal ion speciation, the surface charge of the adsorbent, and the ionization state of functional groups (*e.g.*, COOH, –OH, and $–NH_2$) present on the adsorbent surface.[35] Under acidic conditions, the adsorbent's surface functional groups are protonated, leading to electrostatic repulsion toward metal cations and a reduction in adsorption efficiency. With decreasing pH, abundant H_3O^+ ions compete with metal cations for available surface sites, reducing the adsorption of metal ions. In contrast, at higher pH values, this competition is reduced, resulting in enhanced adsorption of metal ions.[36] However, since metal ions tend to precipitate as hydroxides at very high pH values, it is necessary to determine the optimum pH for adsorption. Therefore, the influence of pH on the recovery of Cd(II), Pb(II), and Ni(II) ions was investigated in the pH range of 2.0–8.0. The results indicated that increasing the pH of the aqueous solution from 2.0 to 6.0 significantly enhanced the recovery efficiencies of Cd(II), Pb(II), and Ni(II) ions, from 17.6% to 98.4%, 57.7% to 95.2%, and 10.2% to 99.9%, respectively. With increasing solution pH, the $CoFe_2O_4$/STWB surface becomes negatively charged, promoting electrostatic attraction toward metal cations and consequently improving adsorption and recovery efficiencies. However, when the pH is increased to 8.0, the recovery efficiencies tend to decrease due to the precipitation of all three metal ions as their hydroxides (Fig. 5). Consequently, the optimum pH for the developed method for the simultaneous quantitative recovery of the analyte ions was identified as 6.0. In a study by Suo *et al.*, which employed a silica-coated magnetic graphene oxide (Fe_3O_4-GO@SiO_2) adsorbent, the optimum pH for Cd(II), Pb(II), and Ni(II) ions was determined to be 5.0, which is in good agreement with the findings of the present study.[36] Similarly, Rajabi *et al.* optimized the solution pH to 6.0 for the simultaneous separation and preconcentration of Cd(II), Cr(VI), Pb(II), Co(II), and Ni(II) ions using a Mg–Al–AHNDA-LDH nanosorbent.[37]

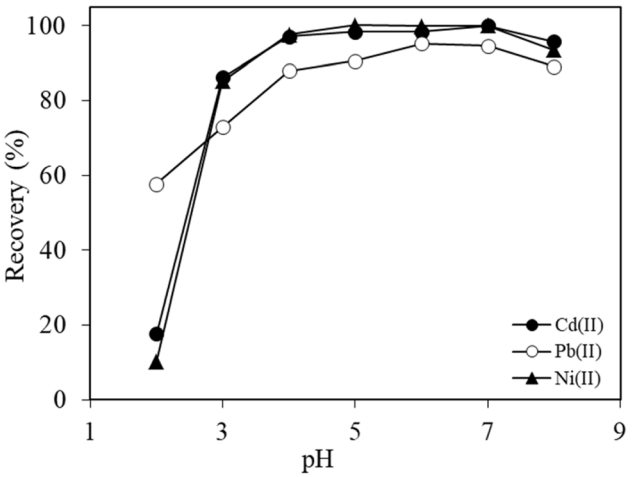

Fig. 5 pH-dependent recovery of analyte ions.

3.2.2 Investigation of the type, concentration, and volume of the desorption solution. The choice of the desorption solution is a key factor for determining the efficient removal of analyte ions from the adsorbent surface. In SPE studies involving the adsorption of metal ions, inorganic acids such as HNO_3 and HCl are generally employed as desorption agents. In an acidic environment, protonation of the functional groups on the adsorbent surface weakens the metal–adsorbent interactions, thereby facilitating the transfer of metal ions into the solution phase.[38] However, the concentration of the desorption solution is also a crucial factor in this process. At low acid concentrations, the interactions between the adsorbent and analyte may not be completely disrupted, resulting in low recovery efficiencies. Conversely, excessively high acid concentrations may damage the functional groups on the adsorbent surface, leading to deterioration of the adsorbent structure.[39] This study investigated the impact of different concentrations of HCl and HNO_3 on the quantitative extraction of analyte ions. The data obtained indicated that both HCl and HNO_3 solutions were effective for the desorption of Cd(II), Ni(II), and Pb(II) ions, and that the recovery of analyte ions increased with increasing concentrations of both acids. Accordingly, HCl was chosen as the desorption solution. The recoveries of Cd(II), Pb(II), and Ni(II) ions were observed to increase from 0.1% to 99.7%, from 0.1% to 100.3%, and from 0.1% to 97.3%, respectively, with increasing the HCl concentration from 0.001 M to 0.2 M (Table

Table 1 Impact of desorption solution type and concentration on recovery efficiency

Concentration (M)	Recovery (%)					
	Cd(II)		Ni(II)		Pb(II)	
	HCl	HNO_3	HCl	HNO_3	HCl	HNO_3
0.001	0.1	0.1	0.1	4.5	0.1	0.1
0.005	82.4	90.2	69.9	75.5	0.1	4.9
0.01	98.8	97.7	86.9	88.4	47.5	43.3
0.05	99.9	99.5	93.7	90.7	94.3	92.5
0.10	101.3	99.5	96.1	94.5	99.9	98.3
0.20	99.7	98.5	97.3	95.7	100.3	98.1
0.30	98.0	99.7	99.2	97.6	100.2	99.4

1). Therefore, 0.2 M HCl was selected as the desorption solution for the simultaneous quantitative recovery of analyte ions.

Optimizing the desorption solution volume is essential for achieving a high preconcentration factor (PF), a key performance indicator of the method. An insufficient eluent volume may hinder the complete transfer of analyte ions from the adsorbent surface to the solution phase, resulting in low recovery, whereas excessive eluent volumes lead to dilution of the analytes and a consequent decrease in the PF. Therefore, in this study, the effect of the volume of the 0.2 M HCl solution, determined as the eluent, on the recovery of the analyte ions was tested over the volume range of 2.5–10.0 mL. When the eluent volume was increased from 2.5 to 5.0 mL, quantitative recovery of the analyte ions was achieved, and no significant improvement was observed at higher eluent volumes. Therefore, an eluent volume of 5.0 mL was selected for all subsequent SPE experiments.

3.2.3 Effect of $CoFe_2O_4$/STWB quantity. The adsorbent dosage is a key parameter influencing the adsorption and recovery efficiencies of the analyte ions, as it determines the active binding sites available for metal ion adsorption in the developed SPE method.[40] When the amount of the adsorbent is insufficient, effective interactions between the analyte ions and the adsorbent surface are limited, resulting in decreased adsorption and recovery efficiency. However, at excessively high adsorbent amounts, problems such as incomplete elution of analyte ions during the desorption step and adsorbent agglomeration may occur.[41] The effect of $CoFe_2O_4$/STWB amount on the recovery of analyte ions was evaluated in the adsorbent amount range of 0.5–3.0 g L^{-1}. As the adsorbent amount was increased from 0.5 g L^{-1} to 2.0 g L^{-1}, the recoveries of Cd(II), Pb(II), and Ni(II) ions increased from 84.3% to 96.8%, from 82.7% to 96.5%, and from 77.1% to 96.2, respectively (Fig. 6).

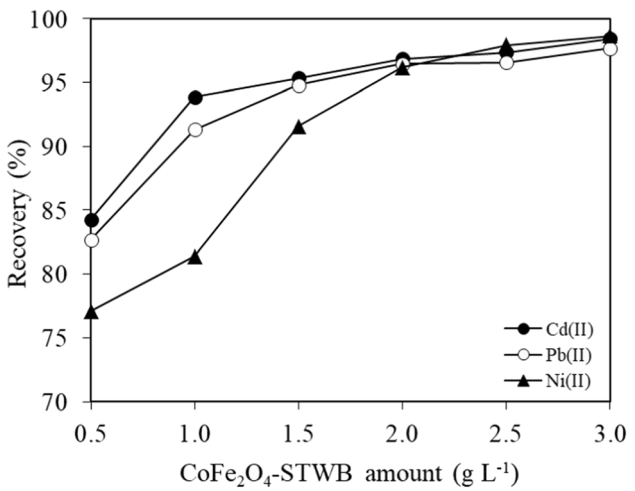

Fig. 6 Influence of $CoFe_2O_4$/STWB quantity on the recovery of analyte ions.

3.2.4 Sample volume effects. Sample volume is a critical parameter directly affecting the PF of the method. To achieve a high PF and thereby enable accurate detection of analytes present at low concentrations, it is essential to identify the maximum sample volume and the minimum eluent volume at which quantitative recovery is achieved.[42] The recovery of Cd(II), Pb(II), and Ni(II) ions was evaluated for sample volumes ranging from 50 to 600 mL using solutions containing 5.0 μg of Cd(II), 20.0 μg of Pb(II), and 10.0 μg of Ni(II) ions, with an adsorbent dosage of 2.0 g L^{-1} $CoFe_2O_4$/STWB. For small sample volumes (up to 50 mL), adsorption and desorption were carried out in polyethylene centrifuge tubes, and $CoFe_2O_4$/STWB was separated from the solution by centrifugation after the extraction process. For larger sample volumes, adsorption was performed in appropriately sized beakers using a magnetic stirrer for the optimized contact time. Following adsorption, the solution was filtered through a 0.45 μm pore-size cellulose nitrate membrane, and $CoFe_2O_4$/STWB containing the adsorbed analyte ions was transferred to polyethylene tubes and treated with 5.0 mL of 0.2 M HCl for desorption. Subsequently, the adsorbent was separated from the solution by centrifugation. The obtained data indicated that the recovery of analyte ions is efficient for sample volumes between 50 and 200 mL. However, when the sample volume was increased from 200 mL to 600 mL, the recoveries of Cd(II), Ni(II), and Pb(II) ions decreased from 97.2% to 89.5%, from 93.4% to 75.1%, and from 95.6% to 80.9%, respectively (Fig. 7). Based on these results, the optimum sample volume for quantitative recovery of analyte ions was found to be 200 mL, and the PF was determined to be 40 when 5.0 mL of the eluent was used.

3.2.5 Adsorption and desorption contact time. The time required for analyte ions to be transferred from the solution phase to the adsorbent surface and to bind to the active adsorption sites is defined as the adsorption equilibrium time. Terminating this period before equilibrium is reached causes a portion of the analyte ions to remain in the solution, resulting in decreased recovery values.[43,44] However, applying unnecessarily long adsorption times not only leads to time and energy consumption but may also cause undesirable effects such as the redistribution of analyte ions back into the solution phase. The impact of adsorption equilibrium time on the adsorption of analyte ions onto $CoFe_2O_4$/STWB was evaluated over a time range of 1–120 min. The experimental results showed that adsorption equilibrium for all three metal ions was achieved in

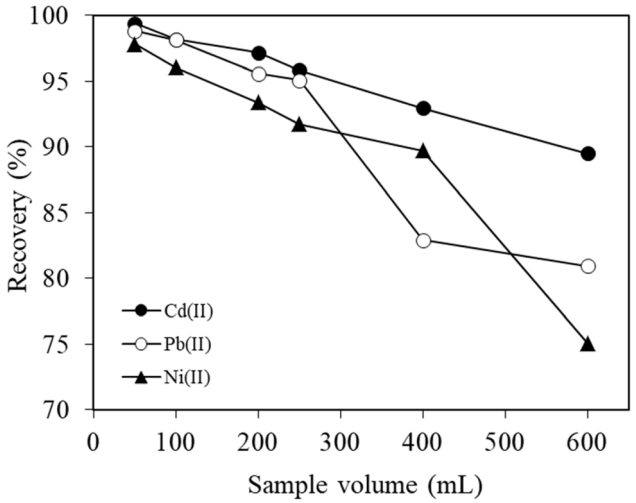

Fig. 7 Effect of sample volume on the extraction efficiency of analyte ions.

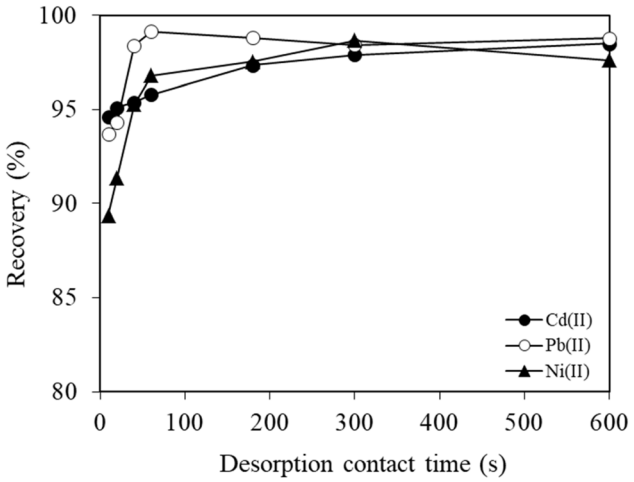

Fig. 8 Influence of contact time on the desorption of analyte ions.

less than 1 min; therefore, an adsorption time of 1 min was used in the following experiments.

The contact time required for the desorption of analyte ions from the $CoFe_2O_4$/STWB surface was investigated over a time range of 10–600 s. For this purpose, solutions adjusted to pH 6.0 and containing 5.0 μg of Cd(II), 20.0 μg of Pb(II), and 10.0 μg of Ni(II) ions were treated with a $CoFe_2O_4$/STWB suspension at a concentration of 2.0 g L^{-1} for 1 min. After the adsorption step, $CoFe_2O_4$/STWB was separated from the medium, and the desorption process was carried out by shaking the adsorbent with 5.0 mL of 0.2 M HCl solution for contact times ranging from 10 to 600 s. Following each contact time, $CoFe_2O_4$/STWB was separated from the solution, and the concentrations of Cd(II), Pb(II), and Ni(II) in the desorption solutions were determined by FAAS. The obtained results demonstrated that desorption occurred within a very short time of approximately 40 s; therefore, a desorption equilibrium time of 1 min was selected for subsequent experiments (Fig. 8).

3.2.6 Effect of interfering ions on the recovery of analyte ions. In SPE studies, coexisting foreign ions may compete with analyte ions for binding to the active adsorption sites on the adsorbent surface, thereby adversely affecting the adsorption process and leading to a decrease in recovery efficiency.[45,46] Therefore, it is important to evaluate the effect of ions that may coexist with analyte ions in real samples on the extraction and determination processes in order to assess the matrix tolerance of the method. For this purpose, known concentrations of various anions and cations were added to 10 mL model solutions containing 5.0 μg of Cd(II), 20.0 μg of Pb(II), and 10.0 μg of Ni(II), and the experiments were carried out under optimum conditions to investigate whether these foreign ions exert any adverse effects on the recovery of the analyte ions. Evaluation of the obtained results revealed that the presence of high concentrations of foreign ions (Na^+, K^+, Ca^{2+}, Mg^{2+}, CO_3^{2-}, NO_3^-, PO_4^{3-}, SO_4^{2-}, NH_4^+, Fe(II), Mn(II), Zn(II), and Hg(II)) in the medium did not cause any significant negative effect on the recovery efficiencies of the analyte ions, and recovery values higher than 90% were achieved for all analytes (Table 2). These findings clearly demonstrate that the developed method exhibits high selectivity and can be applied reliably and successfully even in complex matrices. The observed selectivity can be attributed to the specific interactions between the functional groups present on the adsorbent surface (such as –OH, –COOH, and $–NH_2$) and the target metal ions.[47] These groups facilitate surface complexation and electrostatic

Table 2 Impact of different foreign ions on the recovery of analyte ions

Ions	Conc. (mg L^{-1})	Added as	Cd(II) (recovery%)	Pb(II) (recovery%)	Ni(II) (recovery%)
Na^+	5000	NaCl	93.0 ± 3.1	93.6 ± 1.5	95.7 ± 0.4
K^+	250	KCl	98.8 ± 3.5	97.8 ± 1.6	97.2 ± 4.5
Ca^{2+}	250	$Ca(NO_3)_2$	96.1 ± 0.4	97.8 ± 1.9	97.3 ± 2.4
Mg^{2+}	250	$Mg(NO_3)_2$	97.2 ± 0.9	96.5 ± 2.5	96.7 ± 0.2
CO_3^{2-}	250	Na_2CO_3	93.9 ± 0.1	93.5 ± 0.1	92.3 ± 3.3
NO_3^-	250	$NaNO_3$	98.8 ± 5.3	98.9 ± 2.2	98.4 ± 2.6
PO_4^{3-}	250	Na_3PO_4	95.6 ± 3.6	90.6 ± 0.4	95.6 ± 1.1
SO_4^{2-}	250	Na_2SO_4	94.7 ± 1.7	90.2 ± 2.0	91.4 ± 0.6
NH_4^+	250	NH_4Cl	96.3 ± 0.3	94.1 ± 2.3	94.5 ± 1.3
Fe(II), Mn(II), Zn(II), Hg(II)	25	*	99.2 ± 1.8	100.1 ± 1.6	101.4 ± 0.7

attraction with Cd(II), Pb(II), and Ni(II) ions. Differences in ionic charge density, hydrated ionic radius, and binding affinity also contribute to preferential adsorption of these ions over competing species in complex matrices.[48]

3.2.7 Effect of initial metal ion concentration on analyte adsorption and adsorption isotherms. The influence of the initial metal ion concentration on the adsorption efficiency of Cd(II), Pb(II), and Ni(II) ions onto $CoFe_2O_4$/STWB was evaluated in the concentration range of 10–500 mg L^{-1} for Cd(II) and Ni(II) and 50–500 mg L^{-1} for Pb(II) ions. The obtained results indicated that, with increasing metal ion concentration within the investigated ranges, the amount of metal ions adsorbed per gram of $CoFe_2O_4$/STWB (q_e, mg g^{-1}) increased from 4.7 to 68.8 mg g^{-1} for Cd(II), from 24.4 to 180.8 mg g^{-1} for Pb(II), and from 4.7 to 46.8 mg g^{-1} for Ni(II) ions (Fig. 9). In contrast, the adsorption efficiency (q_e, %) decreased from 93.7% to 27.5%, from 97.8% to 72.3%, and from 93.6% to 18.7% for Cd(II), Pb(II), and Ni(II), respectively. At a fixed $CoFe_2O_4$/STWB dosage, increasing the initial metal ion concentration enhances the concentration gradient between the solution phase and the adsorbent surface, leading to more effective mass transfer and, consequently, an increase in adsorption capacity (q_e, mg g^{-1}). However, as the initial metal ion concentration increases, the active adsorption sites on the adsorbent surface become progressively occupied and eventually reach saturation. Due to the limited number of active sites, not all metal ions can be adsorbed, and a portion remains in the solution phase, resulting in a decrease in adsorption efficiency (q_e, %).[20]

In order to elucidate the adsorbent–adsorbate interactions during the adsorption of analyte ions onto $CoFe_2O_4$/STWB and to gain insight into the surface characteristics of the adsorbent, the experimental data were fitted to the Langmuir and Freundlich isotherm models. The Langmuir isotherm model is based on the assumption that adsorption occurs as a monolayer on a homogeneous adsorbent surface possessing energetically equivalent binding sites, with no interactions between the adsorbed species.[49] In contrast, the Freundlich isotherm model was developed for adsorbents with heterogeneous surfaces and assumes that adsorption takes place in a multilayer manner on active binding sites with different adsorption energies.[50] The linearized equations of the Langmuir and Freundlich isotherm models are given in eqn (1) and (2), respectively.

$$\frac{C_e}{q_e} = \frac{C_e}{q_{max}} + \frac{1}{bq_{max}} \quad (1)$$

$$\ln q_e = \ln K_f + \frac{1}{n}\ln C_e \quad (2)$$

In these equations, q_e denotes the amount of metal ions adsorbed per unit mass of $CoFe_2O_4$/STWB (mg g^{-1}), C_e refers to the metal ion concentration at equilibrium (mg L^{-1}), q_{max} represents the maximum adsorption capacity of $CoFe_2O_4$/STWB

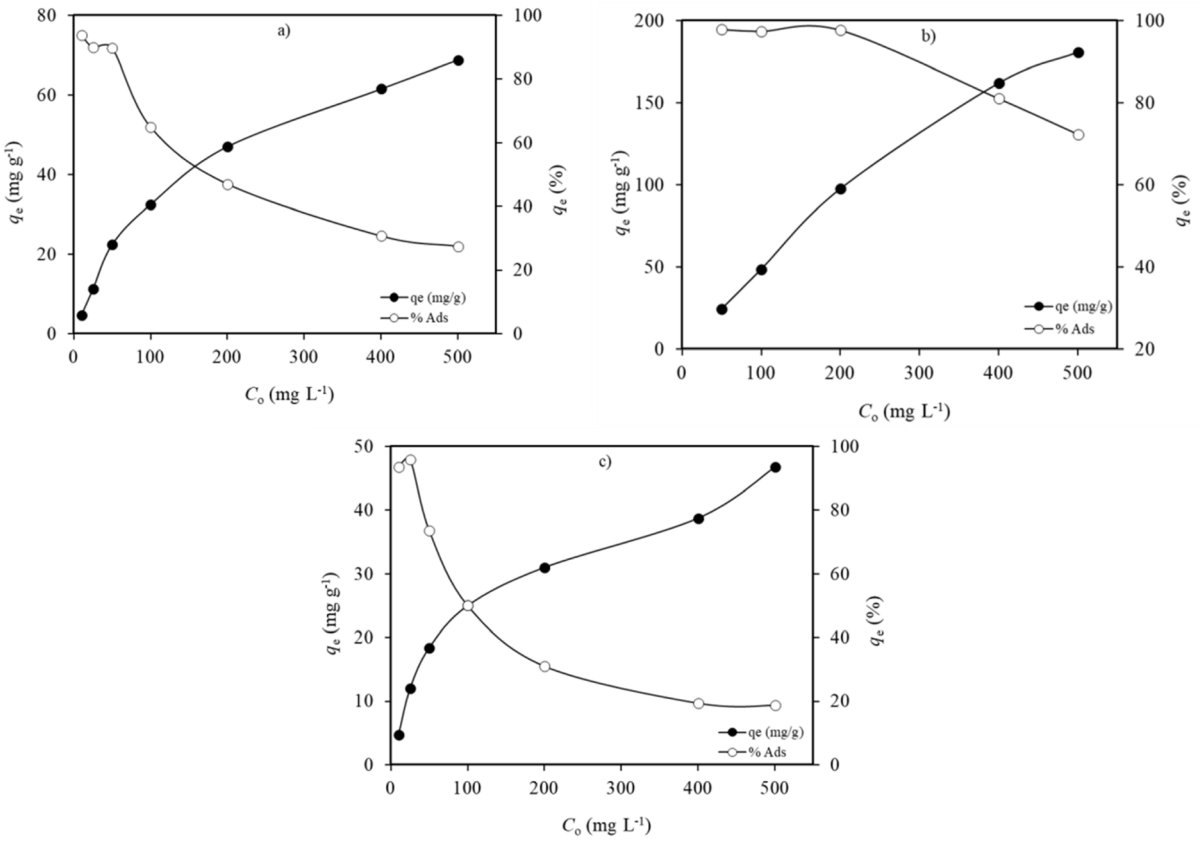

Fig. 9 Impact of initial metal ion concentration on the adsorption of (a) Cd(II), (b) Pb(II) and (c) Ni(II).

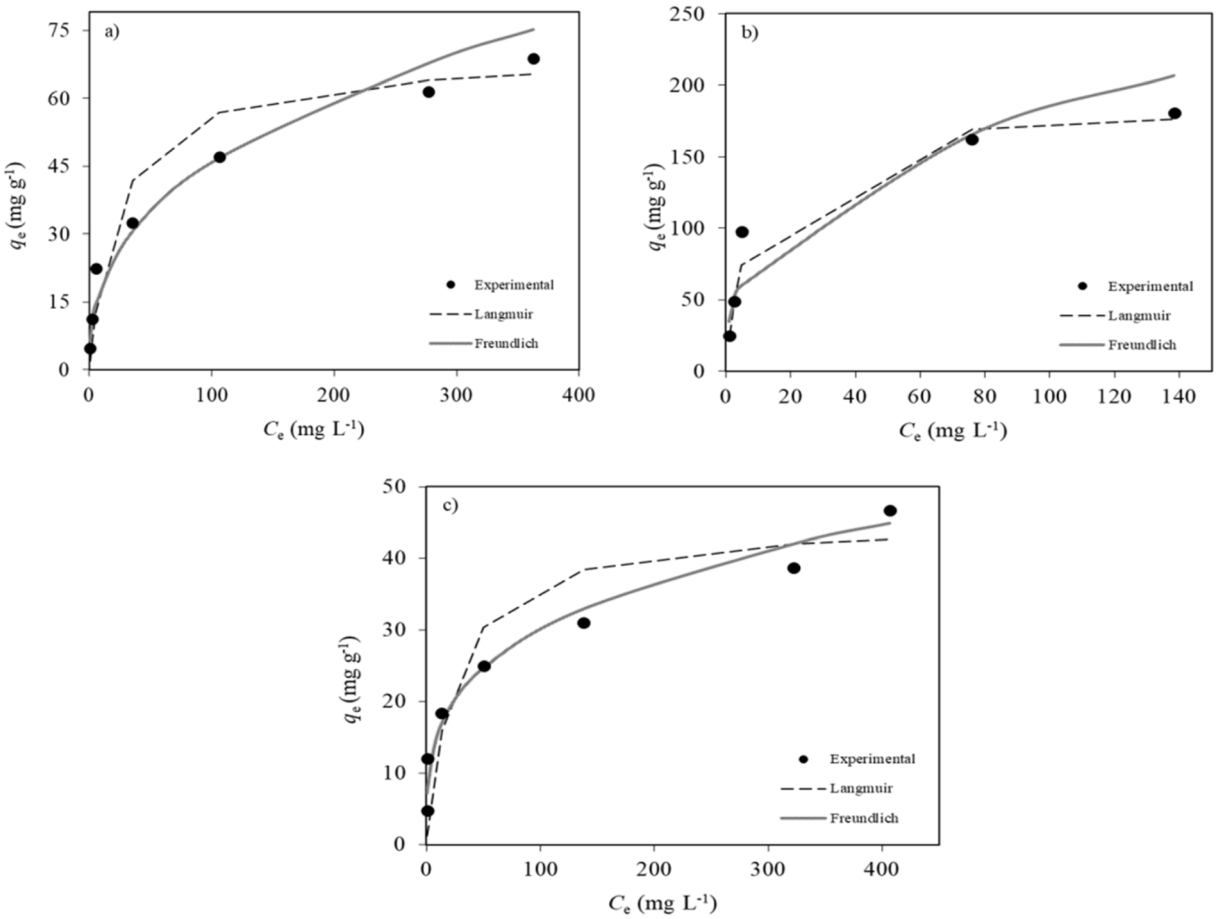

Fig. 10 Non-linear adsorption isotherm models for (a) Cd(II), (b) Pb(II) and (c) Ni(II).

(mg g^{-1}), b is related to the free adsorption energy (L mg^{-1}), K_f is the Freundlich constant related to adsorption capacity (mg g^{-1}), and n is a dimensionless constant related to adsorption intensity. The Langmuir constants b and q_{max} are determined from the linear plot of C_e/q_e *versus* C_e, where the slope and intercept correspond to q_{max} and b, respectively. For the determination of Freundlich constants K_f and n, a linear plot of ln q_e *versus* ln C_e is constructed, where the slope and intercept are used to calculate n and K_f, respectively.

Fig. 10 presents a comparison of the experimental adsorption data with the Langmuir and Freundlich isotherm models for the adsorption of Cd(II), Pb(II), and Ni(II) ions onto $CoFe_2O_4$/STWB. For the adsorption of all three metal ions, the correlation coefficients obtained from the Langmuir isotherm model were higher than those of the Freundlich isotherm model (>0.95), indicating that the adsorption process fits the Langmuir model well. This suggests that the metal ions are adsorbed as a monolayer onto the homogeneous surface of $CoFe_2O_4$/STWB. Using the Langmuir isotherm model, the adsorption capacities of $CoFe_2O_4$/STWB for Cd(II), Pb(II), and Ni(II) ions were calculated to be 69.4 mg g^{-1}, 185.2 mg g^{-1}, and 45.2 mg g^{-1}, respectively. In order to evaluate the effect of $CoFe_2O_4$ modification on the adsorption capacity of STWB, the adsorption capacities of pristine STWB for the metal ions were also determined using the Langmuir isotherm model. According to the obtained results, the adsorption capacities of pristine STWB for Cd(II), Pb(II), and Ni(II) ions were found to be 42.9 mg g^{-1}, 75.8 mg g^{-1}, and 16.8 mg g^{-1}, respectively (Table 3). These findings clearly demonstrate that modification with $CoFe_2O_4$ significantly enhances the adsorption capacity of STWB. Moreover, the adsorption capacity of $CoFe_2O_4$/STWB was found to be higher than that of many adsorbents previously reported in the literature for SPE applications (Table 4).[13,51–56]

To evaluate the suitability of the developed adsorption systems, the dimensionless separation factor, R_L, derived from

Table 3 Isotherm parameters for the adsorption of analyte ions

	Cd(II)	Pb(II)	Ni(II)
Langmuir isotherm model			
q_{max}	69.4	185.2	45.2
b	0.043	0.141	0.041
R^2	0.9847	0.9977	0.9715
Freundlich isotherm model			
K_f	7.73	33.5	8.0
n	2.59	2.71	3.48
R^2	0.9456	0.8638	0.9092

Table 4 Performance comparison of $CoFe_2O_4$/STWB with different adsorbents

Adsorbent	Analyte	Method	Analysis technique	PF	LOD (μg L^{-1})	RSD (%)	Ads. capacity (mg g^{-1})	Ref.
Fe_3O_4@APTES@TX-114[a]	Cd(II)	MSPE[e]	ICP-OES	21	0.889	1.4	9.9	51
MOF[b] (ZIF-8)@ alginate nanocomposite	Cd(II)	μSPE[f]	FAAS	60	3.87	<5	9.1	52
	Ni(II)				7.47		9.4	
Magnetic Fe_3O_4 *Alnus glutinosa* sawdust	Cd(II)	MSPE	FAAS	100	0.62	3.69	80	13
biochar/SiO_2/CTAB[c]	Pb(II)				1.55	3.12	118.5	
Silica nanoparticle-covered GO[d]	Ni(II)	dSPE[g]	FAAS	10	13.5	4.0	—	53
Molybdenum disulfide nanosheets	Cd(II)	SPE	FAAS	71.4	0.37	3.0	10.32	54
	Pb(II)				1.09	4.8	15.04	
	Ni(II)				0.97	4.9	7.40	
Chitosan/thiol functionalized MOF[b]	Pb(II)	SPE	GFAAS	25	0.033	3.9	425.3	55
	Cd(II)				0.008	4.1	109.9	
E. profundum loaded onto Amberlite	Pb(II)	SPE	ICP-OES	80	0.043	4.68	49.83	56
XAD-4	Ni(II)				0.042	4.39	64.35	
$CoFe_2O_4$/STWB	Cd(II)	MSPE	FAAS	40	0.35	1.98	69.4	This work
	Pb(II)				2.67	3.31	185.2	
	Ni(II)				1.83	2.67	45.2	

[a] Fe_3O_4 nanoparticles coated with (3-aminopropyl)triethoxysilane and polyethylene glycol *tert*-octylphenyl ether. [b] Metal organic framework. [c] Cetyltrimethylammonium bromide. [d] Graphene oxide. [e] Magnetic solid phase extraction. [f] Micro solid phase extraction. [g] Dispersive solid phase extraction.

the Langmuir isotherm model and the Freundlich isotherm constant n values can be considered. R_L values in the range of 0–1 and n values between 1 and 10 suggest favorable adsorption behavior.[57] According to the obtained results, the R_L values for Cd(II), Pb(II), and Ni(II) ions in the concentration range of 50–500 mg L^{-1} were found to be 0.32–0.04, 0.12–0.01, and 0.33–0.05, respectively, while the n constants were determined to be 2.59, 2.71, and 3.48, respectively. These results demonstrate that the adsorption of Cd(II), Pb(II), and Ni(II) ions onto $CoFe_2O_4$/STWB is favorable.

3.2.8 Reusability of $CoFe_2O_4$/STWB. The reusability of $CoFe_2O_4$/STWB without regeneration was assessed by contacting 2.0 g L^{-1} of adsorbent suspension with 10.0 μg Cd(II), 50.0 μg Pb(II), and 25.0 μg Ni(II) at pH 6.0. After 1 min of contact time, $CoFe_2O_4$/STWB was separated and subsequently transferred to a fresh metal ion solution. This process was repeated for six consecutive cycles. The results demonstrated that the adsorption efficiency for Cd(II) ions decreased from 99.7% in the first cycle to 81.6% in the fifth cycle. Similarly, the efficiency for Ni(II) declined from 97.9% in the first cycle to 86.8% in the second cycle. In contrast, for Pb(II) it exhibited high stability, retaining an adsorption efficiency of 99.6% even in the sixth cycle (Fig. 11).

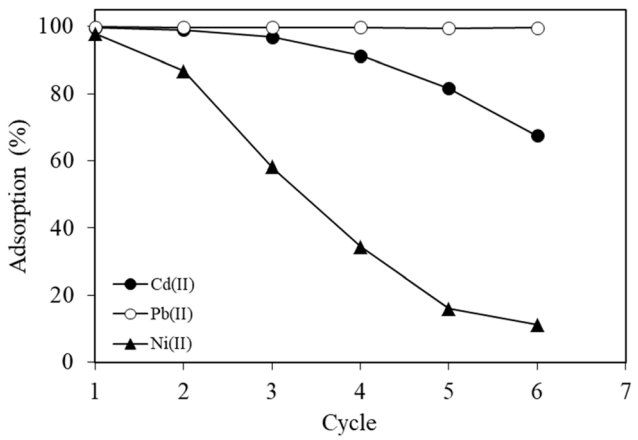

Fig. 11 Reusability of $CoFe_2O_4$/STWB without regeneration.

3.2.9 Adsorption mechanisms of Cd(II), Pb(II), and Ni(II) ions on $CoFe_2O_4$/STWB. The adsorption of Cd(II), Pb(II), and Ni(II) ions on the surface of $CoFe_2O_4$/STWB can be described by a combined mechanism involving electrostatic attraction, surface complexation/coordination, and possible ion-exchange contributions.[59] FTIR analysis confirms the presence of oxygen-containing functional groups on the composite surface. The broad hydroxyl band at 3600–3000 cm^{-1} and the bands observed at approximately 1581 cm^{-1} and 1410 cm^{-1}, commonly attributed to carboxyl/carboxylate-related vibrations, suggest that these functionalities serve as potential coordination sites for divalent metal cations. The Fe–O vibration detected at approximately 567 cm^{-1} confirms the successful

Table 5 Performance characteristics of the $CoFe_2O_4$/STWB-based SPE method

Performance parameters	Analyte ions		
	Cd(II)	Pb(II)	Ni(II)
LOD (μg L^{-1})	0.35	2.67	1.83
LOQ (μg L^{-1})	1.05	8.02	5.50
RSD (%)	1.98	3.31	2.67
PF	40	40	40
Linear range (mg L^{-1})	0.04–2.0	0.30–10.0	0.20–5.0
Correlation coefficient	0.9997	0.9998	0.9998

Table 6 Spike/recovery study of water samples for the SPE method developed using $CoFe_2O_4$/STWB

		Mining wastewater		Stream water		Organized industrial zone wastewater (OIZW)	
Element	Added (μg)	Found (μg)	Recovery (%)	Found (μg)	Recovery (%)	Found (μg)	Recovery (%)
Pb(II)	0	ND[a]	—	ND	—	ND	—
	50.0	46.6 ± 0.1	93.2	47.8 ± 0.5	95.5	44.6 ± 1.1	89.2
	100.0	99.5 ± 0.7	99.5	103.5 ± 0.9	103.5	87.4 ± 0.5	87.4
Cd(II)	0	ND	—	ND	—	ND	—
	10.0	9.72 ± 0.22	97.2	10.1 ± 0.4	101.0	9.21 ± 0.15	92.1
	20.0	20.5 ± 0.4	102.5	18.9 ± 0.3	94.5	17.6 ± 0.1	88.1
Ni(II)	0	ND	—	ND	—	ND	—
	10.0	10.3 ± 0.6	103.0	10.1 ± 0.4	101.0	8.81 ± 0.20	88.1
	20.0	17.6 ± 0.5	88.0	19.0 ± 0.6	95.0	18.3 ± 0.7	91.5

[a] Not detected.

incorporation of $CoFe_2O_4$ within the composite structure. Ferrite-related surface sites may additionally contribute to metal–surface interactions.[60]

The pronounced pH dependence, with high adsorption efficiencies observed at pH 6.0, indicates that partial deprotonation of surface functional groups increases the negative surface charge, thereby enhancing electrostatic interactions with metal ions. Furthermore, the rapid quantitative desorption achieved using 0.2 M HCl suggests that proton competition weakens metal–surface interactions. These findings support a predominantly reversible adsorption process governed by ionic and coordination-type bonding sensitive to pH conditions.

These interaction pathways are likely to remain operative in complex environmental water matrices. The high analytical recoveries obtained from real water samples indicate that the proposed adsorption mechanism remains effective even in the presence of competing ions and dissolved constituents.

3.3 Method validation and applications

3.3.1 Analytical performance of the method. The precision of the proposed method was evaluated by performing ten replicate experiments under the optimized conditions, and the relative standard deviation (RSD%) values were calculated. For each analyte ion, the limit of detection (LOD) was determined as three times the standard deviation of ten blank measurements divided by the PF. Similarly, the limit of quantification (LOQ) was calculated by dividing nine times the standard deviation by the PF. The PF for each analyte was determined by dividing the optimum sample volume (200 mL) by the final volume (5.0 mL).

Table 7 Quantification of heavy metals in actual water matrices

Element	Mining wastewater (μg L^{-1})	Stream water (μg L^{-1})	OIZW (μg L^{-1})
Pb(II)	GSA	20.9 ± 0.8	GSA
Cd(II)	2.81 ± 0.02	GSA	GSA
Ni(II)	8.32 ± 0.30	7.21 ± 0.18	6.19 ± 0.14

Table 5 summarizes the analytical performance parameters of the developed method. These results were further compared with those of other SPE procedures reported in the literature, as shown in Table 4. The $CoFe_2O_4$/STWB based SPE method exhibits lower RSD% and LOD values, as well as a higher PF, compared to many previously reported methods.

3.3.2 Method accuracy and application to real sample matrices. The accuracy and precision of the developed SPE method were evaluated by spiking 50 mL of mining wastewater, stream water, and organized industrial zone wastewater samples with different concentrations of HM ions. Based on the results obtained, the recovery efficiencies of Cd(II), Pb(II), and Ni(II) ions were determined to be in the ranges of 88.1–102.5%, 87.4–103.5%, and 88.0–103.0%, respectively (Table 6). These results demonstrate that the proposed method can be effectively used for water samples without significant matrix effects. Finally, the developed method was implemented to determine the concentration of Cd(II), Pb(II), and Ni(II) ions in the aforementioned water samples (Table 7).

4 Conclusion

In this study, spent tea waste biochar was magnetically modified with $CoFe_2O_4$ and the performance of the adsorbent for the separation and preconcentration of Cd(II), Pb(II), and Ni(II) ions from mining wastewater, stream water, and wastewater samples collected from an organized industrial zone was comprehensively evaluated using the SPE method. The findings reveal that magnetic modification of spent tea waste with $CoFe_2O_4$ markedly enhances the performance characteristics of the adsorbent. The incorporation of $CoFe_2O_4$ promotes more effective binding mechanisms for heavy metal ions, leading to high adsorption efficiencies for Cd(II), Pb(II), and Ni(II). In particular, the pronounced increase in adsorption capacity for Pb(II) clearly indicates that $CoFe_2O_4$ modification strengthens heavy metal–surface interactions. The developed SPE method is distinguished by extremely short equilibrium times, rendering it highly advantageous in terms of time and energy efficiency, as both adsorption and desorption processes are completed within seconds. Furthermore, the magnetic properties of the

adsorbent enable its rapid and facile separation from the medium, representing a significant advantage that enhances the practicality and ease of application of the method. From an analytical perspective, the developed method provides a reliable and robust approach for trace level heavy metal determination, characterized by low LODs, high PF, and satisfactory precision. The effective performance of the method in complex water matrices demonstrates its robustness against matrix effects and confirms its suitability for real sample analysis.

In conclusion, this study demonstrates that a widely available and cost-effective waste material can be successfully transformed into a high-value adsorbent material, thereby providing a meaningful contribution to environmental sustainability. With its economical, environmentally friendly, and high-performance characteristics, $CoFe_2O_4$-modified spent tea waste can be regarded as a viable alternative adsorbent for heavy metal monitoring in environmental water samples.

Author contributions

SS: design of methodologies, investigation, data curation and analysis. DO: supervision, resources, design of methodologies, writing – review & editing, conceptualization. CD: writing – review & editing, methodology, formal analysis, conceptualization.

Conflicts of interest

The authors declare that they have no known competing financial interests or personal relationships that could have appeared to influence the work reported in this paper.

Data availability

The data that support the findings are within the paper and additional data are available from the corresponding author upon reasonable request.

Acknowledgements

This work was supported by Gümüşhane University, Scientific Research Projects Coordination Department (Project Number: 23.E0116.07.01). The authors would also like to thank Dr Yunus Önal for his valuable assistance in carrying out the BET surface area analysis measurements.

References

1 H. Ali, E. Khan and I. Ilahi, *J. Chem.*, 2019, **2019**, 6730305.
2 R. M. Madjar and G. Vasile Scăeţeanu, *Sustainability*, 2025, **17**(16), 7368.
3 A. Bernard, *Indian J. Med. Res.*, 2008, **128**(4), 557–564.
4 C. Gundacker, M. Forsthuber, T. Szigeti, R. Kakucs, V. Mustieles, M. F. Fernandez, E. Bengtsen, U. Vogel, K. S. Hougaard and A. T. Saber, *Int. J. Hyg. Environ. Health*, 2021, **238**, 113855.
5 G. Genchi, A. Carocci, G. Lauria, M. S. Sinicropi and A. Catalano, *Int. J. Environ. Res. Public Health*, 2020, **17**(3), 679.
6 L. D. Nguyen, C. T. G. Hua, T. X. H. Dao and P. H. Tran, *Microchem. J.*, 2025, **215**, 114530.
7 J. Ruenjaiman, D. Sroichot, K. Kaewjua, W. Siangproh and K. Songsrirote, *Microchem. J.*, 2026, **220**, 116610.
8 A. A. Zendehdel, S. M. Sorouraddin and M. A. Farajzadeh, *Anal. Methods*, 2024, **16**(11), 1593–1602.
9 Y. Liu, L. Xu, J. Liu and X. Liu, *Anal. Methods*, 2015, **7**(24), 10151–10161.
10 M.-M. Zhao, H.-Z. Wu, X.-K. Deng, R.-N. Yi and Y. Yang, *Anal. Methods*, 2023, **16**(3), 333–343.
11 C. Özdemir, S. Saçmaci and Ş. Kartal, *Anal. Methods*, 2013, **5**(16), 3977–3983.
12 R. R. Pasupuleti and Y.-L. Huang, *J. Chin. Chem. Soc.*, 2023, **70**(6), 1326.
13 C. Duran and D. Ozdes, *Int. J. Environ. Anal. Chem.*, 2023, **103**(16), 4857–4875.
14 P. Montoro-Leal, J. C. García-Mesa, M. T. Siles Cordero, M. M. López Guerrero and E. Vereda Alonso, *Microchem. J.*, 2020, **155**, 104796.
15 R. N. Avcı, T. Oymak and E. Bağda, *Anal. Lett.*, 2022, **55**(16), 2495–2506.
16 B.-M. Jun, J.-Y. Jung, M. Oh, H.-C. Eun, S. Moon, H. Rho, K. Chon, S.-N. Nam and Y. Yoon, *J. Water Process Eng.*, 2025, **75**, 107956.
17 D. Ozdes and C. Duran, *Environ. Monit. Assess.*, 2021, **193**, 642.
18 G. Yang, J. Zhang, J. Zhang, P. Wang, W. Xia, J. Wang, X. Shen and C. Kong, *Food Chem.*, 2025, **492**, 145390.
19 Z. Niu, Y. Ma, M. Ma, Z. Tang and Y. Wen, *Microchem. J.*, 2025, **212**, 113275.
20 C. Duran, S. T. Ozeken, S. Seker and D. Ozdes, *Gels*, 2025, **11**, 628.
21 S. Gitipour, M. Sanaei, R. Lak and A. Karbassi, *Sci. Rep.*, 2025, **15**, 7912.
22 J. Li, M. Zhang, Q. Kong, T. Zeng, Y. Mao, J. Liu and S. Xie, *J. Taiwan Inst. Chem. Eng.*, 2025, **166**(2), 105532.
23 S. I. S. Al-Hawary, A. Kamel, S. S. Abdullaev, A. K. Kareem, K. A. Alkhuzai, R. M. Romero-Parra, A. H. Amini, T. Alawsi, M. Abosaooda and M. Dejaverdi, *Alex. Eng. J.*, 2023, **74**, 737–749.
24 F. Lin, J. Zeng, J. Chen, S. Li and W. Lin, *Int. J. Biol. Macromol.*, 2025, **325**, 147071.
25 M. H. Ullah and M. J. Rahman, *Heliyon*, 2024, **10**(17), e36869.
26 G. Yin, X. Chen, B. Sarkar, N. S. Bolan, T. Wei, H. Zhou and H. Wang, *Chem. Eng. J.*, 2023, **466**, 143199.
27 N. Shabelskaya, M. Egorova, A. Radjabov, M. Burachevskaya, I. Lobzenko, T. Minkina and S. Sushkova, *Water*, 2023, **15**(1), 93.
28 C. Lai, F. Huang, G. Zeng, D. Huang, L. Qin, M. Cheng, C. Zhang, B. Li, H. Yi, S. Liu, L. Li and L. Chen, *Chemosphere*, 2019, **224**, 910–921.
29 Y. I. E. Aboulsoud, *Environ. Dev. Sustain.*, 2024, **27**(7), 16451–16468.

30 S. Fan and L. Zhang, *Biomass Convers. Biorefin.*, 2021, **11**(5), 1719–1732.
31 N. Zhang, F. Reguyal, S. Praneeth and A. K. Sarmah, *Sci. Total Environ.*, 2023, **886**, 163923.
32 S. Fan, J. Tang, Y. Wang, H. Li, H. Zhang, J. Tang, Z. Wang and X. Li, *J. Mol. Liq.*, 2016, **220**, 432–441.
33 T. N. Mashoene, A. L. Taka, S. O. Akpotu, I. A. Lawal and M. J. Klink, *Appl. Sci.*, 2023, **13**(13), 7493.
34 D. H. K. Reddy and S.-M. Lee, *Colloids Surf., A*, 2014, **454**, 96–103.
35 E. Parandi, M. Shirani, Z. S. Korrani, M. Teimouri, M. A. Poor, H. Sadatfaraji, Z. Sarlak and S. Shafiei, *Emergent Mater.*, 2025, **8**, 4321–4335.
36 L. Suo, X. Dong, X. Gao, J. Xu, Z. Huang, J. Ye, X. Lu and L. Zhao, *Microchem. J.*, 2019, **149**, 104039.
37 M. Rajabi, S. Arghavani-Beydokhti, B. Barfi and A. Asghari, *Anal. Chim. Acta*, 2017, **957**, 1–9.
38 S. M. M. Attaf, R. Alotaibi, A. A. Alotaibi and S. M. A. Azeem, *J. Food Compos. Anal.*, 2025, **137**, 106883.
39 M. S. Yalçın, S. Özdemir, E. Kılınç and M. Soylak, *J. Food Compos. Anal.*, 2024, **134**, 106561.
40 H. E. H. Ahmed, A. M. A. Mohammed and M. Soylak, *Water, Air, Soil Pollut.*, 2026, **237**, 261.
41 H. Akbiyik, A. Girgin, B. T. Zaman, A. Atakol, N. San and S. Bakirdere, *J. Anal. Sci. Technol.*, 2025, **16**, 23.
42 H. E. H. Ahmed, O. Ozalp and M. Soylak, *J. Food Compos. Anal.*, 2023, **118**, 105163.
43 M. B. Arain and M. Soylak, *Food Chem.*, 2025, **471**, 142766.
44 M. Soylak, A. A. Isak and O. Ozalp, *J. Food Compos. Anal.*, 2025, **148**(3), 108401.
45 A. Türker and O. Acar, *Food Anal. Methods*, 2025, **18**, 2106–2119.
46 M. Ahmad, A. Badshah, H. Li, M. Asad, M. A. Ibrahim, E. A. Ali, A. A. Shahat, U. Nishan, M. Khan and W. Sun, *J. Sep. Sci.*, 2024, **47**, e70004.
47 X. Tan, Y. Liu, G. Zeng, X. Wang, X. Hu, Y. Gu and Z. Yang, *Chemosphere*, 2015, **125**, 70–85.
48 M. Suppapruek, P. Threepopnatkul, A. Sittattrakul and W. Lerdwijitjarud, *E3S Web of Conferences*, 2021, vol. 302, p. 02020.
49 I. Langmuir, *J. Am. Chem. Soc.*, 1918, **40**, 1361–1403.
50 H. M. F. Freundlich, *Z. Phys. Chem.*, 1906, **57**, 385–470.
51 C. Caner, M. Yogurtcuoglu Ciftci, S. Tabassum, H. Altundag and E. Bulut, *J. Mol. Struct.*, 2025, **1321**(1), 139836.
52 M. Soylak, M. Alparslan and O. Ozalp, *Anal. Lett.*, 2026, **59**(6), 993–1011.
53 K. Seval and A. Akdoğan, *Int. J. Environ. Anal. Chem.*, 2022, **102**(19), 8402–8418.
54 Z. Tamoradi Babaei, A. Larki and K. Ghanemi, *J. Iran. Chem. Soc.*, 2022, **19**, 95–107.
55 L. Huang, W. Huang, R. Shen and Q. Shuai, *Food Chem.*, 2020, **330**, 127212.
56 S. Ozdemir, E. Kılınç, Ö. Acer and M. Soylak, *Microchem. J.*, 2021, **171**, 106758.
57 S. T. Ozeken, D. Ozdes and C. Duran, *J. Anal. Sci. Technol.*, 2025, **16**, 22.
58 B. Zhao, X. Xu, R. Zhang and M. Cui, *Environ. Sci. Pollut.*, 2021, **28**, 16408–16419.
59 Z. Abbas, S. Ali, M. Rizwan, I. E. Zaheer, A. Malik, M. A. Riaz, M. R. Shahid, M. Z. U. Rehman and M. I. Al-Wabel, *Arab. J. Geosci.*, 2018, **11**(16), 448.
60 H. Chakhtouna, H. Benzeid, N. Zari, A. E. K. Qaiss and R. Bouhfid, *Sep. Purif. Technol.*, 2021, **266**, 118592.